analytical chemistry

pubs.acs.org/ac Article

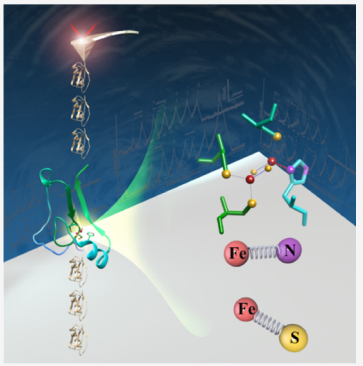
Single-Molecule Force Spectroscopy Reveals that the Fe−N Bond Enables Multiple Rupture Pathways of the 2Fe2S Cluster in a MitoNEET Monomer

Guobin Song, Xuan Ding, Huaxing Liu, Guodong Yuan, Fang Tian, Shengchao Shi, Yang Yang, Guoqiang Li, and Peng Zheng*

Cite This: *Anal. Chem.* 2020, 92, 14783−14789 Read Online

ACCESS | Metrics & More | Article Recommendations | Supporting Information

ABSTRACT: The mitochondrial outer membrane protein, mitoNEET (mNT), is an iron−sulfur protein containing an $Fe_2S_2(His)_1(Cys)_3$ cluster with a unique single Fe−N bond. Previous studies have shown that this Fe(III)−N(His) bond is essential for metal cluster transfer and protein function. To further understand the effect of this unique Fe−N bond on the metal cluster and protein, we used atomic force microscopy-based single-molecule force spectroscopy (AFM-SMFS) to investigate the mechanical unfolding mechanism of an mNT monomer, focusing on the rupture pathway and kinetic stability of the cluster. We found that the Fe−N bond was the weakest point of the cluster, the rupture of which occurred first, and could be independent of the cluster break. Moreover, this Fe−N bond enabled a dynamic and labile iron−sulfur cluster, as multiple unfolding pathways of mNT with a unique $Fe_2S_2(Cys)_3$ intermediate were observed accordingly.



INTRODUCTION

An iron−sulfur protein is an ancient yet ubiquitous type of metalloprotein existing in nature, which plays a critical role in living organisms.[1,2] Recently, a new family of 2Fe2S proteins, NEET, was discovered, which involves mitochondrial iron and reactive oxygen species homeostasis.[3,4] The first discovered human mitoNEET (mNT) is identified as a drug target for insulin resistance-lowering drug.[5] These functions are related to its unique $Fe_2S_2(His)_1(Cys)_3$ cluster coordinated by a single histidine and three cysteine residues.[3,6,7] Previous studies have shown that this unique iron−histidine interaction (Fe(III)−N(His) bond) in the cluster is critical for these functions, especially for metal cluster transfer. When this histidine is mutated or bound, the cluster transferability of mNT to other acceptor proteins is inhibited.[6]

To further understand the effect of this labile Fe−N bond on these iron−sulfur clusters and the NEET proteins, we studied the mechanical unfolding process of an mNT monomer in its oxidized form by atomic force microscopy-based single-molecule force spectroscopy (AFM-SMFS) (Figure 1A). mNT is an integral protein of the mitochondrial outer membrane, whose structural, biochemical, and spectroscopic properties have been characterized using classical methods over the past decade. The full-length mNT contains 108 amino acids (aa). Most studies have concentrated on the 76 aa-length soluble form (residues 33−108), which is also used here. The X-ray crystal structure shows that the protein is present as a dimer, with each monomer folding into two spatially different parts: a three-strand β-sheet domain (residues 56−61, 68−71, and 98−104) and an α-helical metal cluster-binding domain (residues 72−87) (Figure S1).[5,8] The unique feature of mNT is that the 2Fe2S cluster is coordinated by one imidazole nitrogen from a histidine residue (His87) and three cysteinyl sulfurs (Cys72, Cys74, Cys83) (Figure 1B). Due to this cluster, the protein is red-colored in solution and displays a unique UV−vis absorption spectrum, with a peak at 458 nm (Figure S2).

Here, single-molecule force spectroscopy was used to study the unfolding process of the mNT monomer. This technique, including optical tweezers, magnetic tweezers, and single-molecule atomic force microscope, allows the stretching of one molecule at a time to induce breaking of inter- or intramolecular bonds/interactions.[9−17] As a result of its high applied force range, AFM is suitable for studying protein (un)folding,[18−27] protein−ligand (protein) interactions,[28−33] and chemical bonds.[34−43] It can induce the protein unfolding and stable metal cluster rupture in complex metalloprotein systems.[44−51] Thus, we used AFM to study the rupture

Received: August 19, 2020
Accepted: September 25, 2020
Published: October 13, 2020



Downloaded via NANJING UNIV on July 12, 2021 at 08:28:07 (UTC).
See https://pubs.acs.org/sharingguidelines for options on how to legitimately share published articles.

© 2020 American Chemical Society

https://dx.doi.org/10.1021/acs.analchem.0c03536
Anal. Chem. 2020, 92, 14783−14789

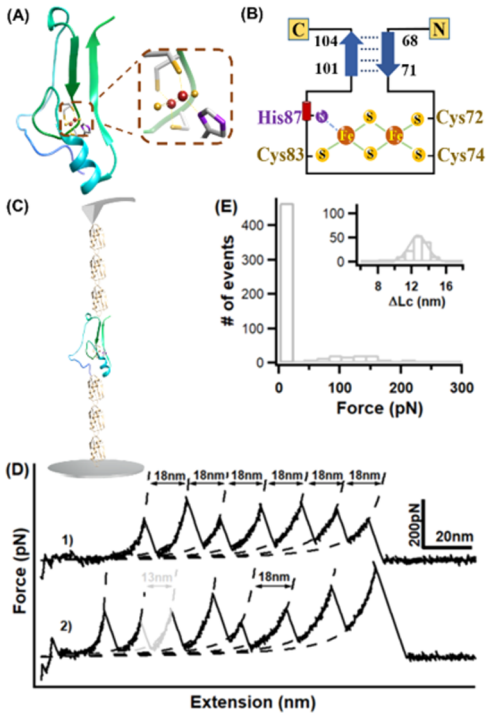


Figure 1. Predicted structure (A) and schematic (B) of the mNT monomer showing the two β-strand motif and the metal cluster-binding domain based on the mNT dimer (PDB: 2QH7). The 2Fe2S cluster is enlarged. (C) Setup of an AFM-SMFS experiment showing how mNT is stretched using a $(GB1)_3$-mNT-$(GB1)_3$ construct. (D) Force–extension curves of polyprotein unfolding displaying two different patterns: most curves (curve 1) show peaks only from GB1 with a ΔL_c of 18 nm, and 25% show an additional peak with a ΔL_c of 13 nm (curve 2) from the unfolding of apo-mNT. (E) Force histogram showing that most apo-mNT have a low unfolding force below the detection limit of AFM (15 pN). The inset is the ΔL_c histogram of apo-mNT.

mechanism and kinetic stability of this iron–sulfur cluster in mNT.

RESULTS AND DISCUSSION

To study the unfolding of mNT unambiguously by AFM-SMFS, a polyprotein construct, $(GB1)_3$-mNT-$(GB1)_3$, was prepared. Mass spectroscopy measurements of the polyprotein showed an expected molecular weight of ~50 kDa (Figure S3). Here, one mNT is flanked by three marker proteins, GB1, which has been well characterized with a ΔL_c of 18 nm and an unfolding force of 180 pN. It serves as a single-molecule fingerprint and force caliper (Figure 1C). Thus, only a force–extension curve with at least four GB1 unfolding events was selected and analyzed, ensuring the detection of the sandwiched mNT.[52] Its gel filtration profile showed only one peak eluted at 8.4 mL, indicating a monomer state of mNT present in the polyprotein construct (Figure S4). The adjacent protein GB1 may inhibit mNT dimer formation due to steric hindrance. Nevertheless, the UV–vis spectrum of the polyprotein, which only comes from the 2Fe2S cluster of mNT, showed an identical signal to that of the mNT dimer (Figure S2). Thus, our polyprotein construct can be a suitable sample to study the unique 2Fe2S cluster in mNT. The mNT monomer structure is predicted based on the dimer structure (PDB: 2QH7), in which a two β-strand motif (residues 68–71, 101–104) may be present (Figures 1B, and S1).

We first studied mNT without the 2Fe2S cluster (apo-mNT) as a control, which was prepared by standard protocols (Figure S2). When stretched using a single-molecule atomic force microscope, 75% of the force–extension curves of the polyprotein showed unfolding force peaks only from marker protein GB1 (Figure 1D, curve 1, n = 467), while 25% showed an additional force peak (curve 2) with a ΔL_c of ~13 nm (n = 170,12.3 ± 1.4 nm, average ± standard deviation, Figure 1E, inset), fitted using the worm-like chain (WLC) model of polymer elasticity.[53] This length corresponds to the unfolding and extension of a protein fragment of ~36 amino acids (the length of the backbone for one aa is 0.36 nm, 13 nm/0.36 nm/aa = 36.1 aa). Based on the structure of mNT (Figure 1B), this force peak was most likely from the unfolding of the two β-strand motif (residues 68–71, 101–104, 37 aa in between), the only possible structured protein fragment in the monomer. Its theoretical ΔL_c is 0.36 nm/aa × 37 aa − 0.46 nm = 12.9 nm (0.46 nm is the distance between residues 68 and 104 in the folded mNT). However, the majority of apo-mNT did not show this peak. One possibility is such a small β-strand motif with four hydrogen bonds is only transitionally stable in the apo form. Another explanation is that a large fraction of apo-mNT is incorrectly folded. Circular dichroism (CD) experiments on apo and holo-mNT also corroborate these two explanations. The CD signal in apo-mNT is weaker than that of holo-mNT from wavelength 205 to 230 nm, indicating a less secondary structure of apo-mNT (Figure S5).

Next, we focused on holo-mNT containing the 2Fe2S cluster. In comparison with apo-mNT, the first difference was that most curves showed detectable mNT unfolding peak(s). For example, holo-mNT showed more frequent unfolding events with the ΔL_c of 13 nm (12.5 ± 1.3 nm, n = 412, 42%, Figure 2A, curves 1 and 2 and Figure 2B) and an average force of 105 ± 93 pN (Figure 2C). In addition, a stepwise mNT unfolding peak with a cumulative ΔL_c of 13 nm was detected (curve 3, n = 183, 18%). The ΔL_c of the first peak was 8 nm, which agreed with the unfolding of the two β-strand motif and the extension of residues outside the metal cluster (7.8 ± 0.9 nm, residues 68–72 and 88–104, (5 + 17) aa × 0.36 + 0.46 − 0.5 = 7.9 nm). The force was 87 ± 79 pN (Figure 2D). The second peak had a ΔL_c of 5 nm, which agreed with the rupture of the 2Fe2S cluster (5.2 ± 1 nm, residues 72–87, 15 aa × 0.36 − 0.5 = 4.9 nm).

It is noteworthy that the 5 nm peak was not observed in apo-mNT, indicating that the incorporation of the metal cluster stabilizes the whole protein structure and an unfolding intermediate. Moreover, a single force peak with a ΔL_c of 5 nm only from the rupture of the metal cluster was also observed (Figure 2A, curves 4 and 5, n = 248, 25%) with a rupture force of 82 ± 51 pN (Figure 2E).

In addition to the observation of a one-step rupture of the cluster, stepwise rupture of the 2Fe2S cluster was detected, as shown by stepwise peaks with a cumulative ΔL_c of 5 nm (Figure 3, curves 2 and 3). Here, the first force peak with a ΔL_c of 2 nm (5 aa × 0.36 = 1.8 nm) agreed with the rupture of the single Fe–N(His87) bond, which stops at Fe–S(Cys83), leading to a partially ruptured $Fe_2S_2(Cys)_3$ intermediate. Then, the break of the intermediate leads to a force peak with a ΔL_c of 3 nm (10 aa × 0.36 − 0.5 = 3.1 nm). This conclusion is further supported by the observation of a stepwise peak with a first 10 nm peak followed by the 3 nm peak (curve 4) and the observation of a single 3 nm peak (curves 5 and 6). Here, the 10 nm peak comes from the simultaneous unfolding of the two

https://dx.doi.org/10.1021/acs.analchem.0c03536
Anal. Chem. 2020, 92, 14783–14789

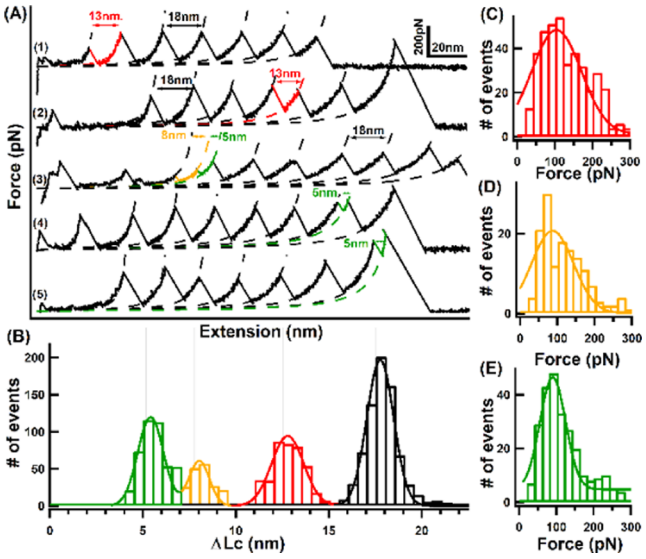


Figure 2. (A) Representative curves of holo-mNT showing three different unfolding pathways involving the rupture of the intact $Fe_2S_2(His)_1(Cys)_3$ cluster: a single peak with a ΔL_c of 13 nm from the one-step unfolding of mNT (curves 1 and 2, colored in red); a stepwise peak with a cumulative ΔL_c of 13 nm from the sequential unfolding of the two β-strand motif and the metal cluster (curve 3, colored in yellow for 8 nm and green for 5 nm); and a single peak with a ΔL_c of 5 nm from the metal cluster rupture (curves 4 and 5). (B) ΔL_c histogram showing the three different peaks. Force histograms are shown for mNT (C), the 8 nm peak (D), and the cluster (E).

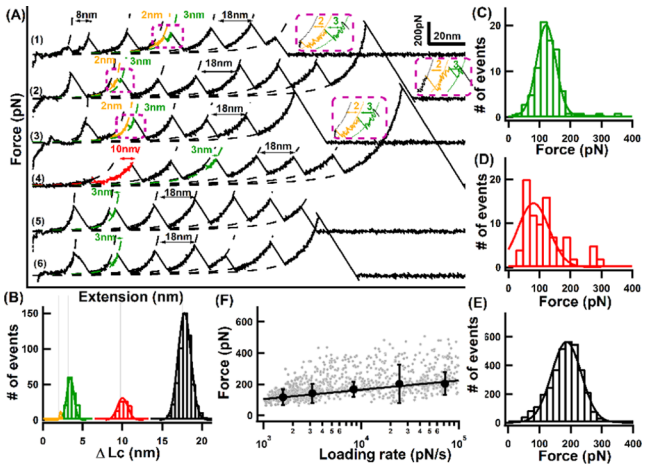


Figure 3. (A) Representative curves are shown for four different unfolding scenarios involving the stepwise rupture of the cluster: 2 nm peaks (yellow) from the break of the single Fe−N bond (residues 83−87); 3 nm peaks (green) from the partially ruptured $Fe_2S_2(Cys)_3$ cluster; and 10 nm peaks (red) from the rupture of the two β-strand motif and the Fe−N bond. (B) ΔL_c histogram confirming the three populations. Histograms showing the rupture force distribution for the $Fe_2S_2(Cys)_3$ cluster (C), the 10 nm peak (D), and GB1 (E). (F) Plot between the loading rate and the cluster rupture force (5 nm peak) showing a linear dependency. The result can be fitted by a Δx of 0.16 nm and an off rate of 0.68 s^{-1}.

β-strand motif (8 nm) and the Fe−N(His87) bond (2 nm). The average unfolding force for the 3 nm peak is 111 ± 43 pN. More curves are provided in the Supporting Information (Figure S6).

Finally, we performed an AFM unfolding experiment on mNT under different pulling speeds to extract the cluster kinetics.[54] The rupture force of the intact 2Fe2S cluster (5 nm peak) and its corresponding loading rate is plotted (Figures 3F and S9). Similar to protein unfolding, the rupture force of the cluster is dependent on the loading rate. The data points can be fitted by a linear line, and a Δx of 0.16 nm and an off rate of 0.68 s^{-1} were obtained based on the Bell−Evans model.

Here, we used AFM-SMFS to investigate the unfolding process of the mitoNEET (mNT) protein, which contains a unique $Fe_2S_2(His)_1(Cys)_3$ cluster. First, our work demonstrates that the incorporation of the metal cluster stabilizes the protein, as only 25% of the unfolding event of apo-mNT (13 nm peak) was detectable while 70% of holo-mNT was detected (13 nm peak: 42%; 8 + 5 nm-peak: 18%, 10 + 3 nm peak 10%, Table 1). Also, AFM experiments on both apo and holo-mNT

Table 1. Data Summary for Each Holo-mNT Unfolding Scenario

mode	ΔL_c (nm)	%
13	12.5 ± 1.3	42
8 + 5	7.8 ± 0.9	18
5	5.2 ± 1	25
8 + 2 + 3		0.5
2 + 3	2.1 ± 0.3	0.5
10 + 3	9.8 ± 0.9	10
3	3.1 ± 0.7	4

monomers provide structural information about the protein. Since only the mNT dimer structure is available, it is unknown whether the two β-strand motif is still present in the monomer. Our detection of 13 nm peak, 8 nm peak, and 10 nm peak suggested the formation of this motif in the mNT monomer, and holo-mNT was more structured than the apo one, which was further supported by the CD results. Nevertheless, our theoretical ΔL_c calculation of each mNT monomer unfolding/rupture event is based on the dimer structure. Thus, may be some degree of inaccuracy is present and future work on the mNT dimer is necessary to confirm our calculations.

More importantly, our results revealed the dynamics and lability of the $Fe_2S_2(His)_1(Cys)_3$ cluster in holo-mNT. In total, three different types of mNT unfolding pathways were observed, such as one, two, and three-step unfolding scenarios (Figure 4). The first is the one-step unfolding of mNT (42%, pathway 1, P1, Table 1) with a 13 nm peak in which protein unfolding and metal cluster rupture are coupled. The second pathway (43%, P2, P2′) involves a complete metal cluster as an unfolding intermediate. Here,18% (P2) of mNT showed a two-step unfolding with the first 8 nm peak from the two β-strand motif and a second 5 nm peak from the metal cluster. Also, 25% (P2′) of events showed only the second 5 nm peak from the cluster. Finally, a three-step mNT unfolding pathway (15%, P3, P3′, P3″, and P3‴) involves a partially ruptured $Fe_2S_2(Cys)_3$ intermediate whose rupture leading to a 3 nm peak was observed. In total, seven different unfolding scenarios with two intermediates were observed, revealing the dynamic unfolding pathways of the mNT monomer under mechanical manipulation.

The key finding of the present study perhaps is a partially ruptured metal cluster intermediate $Fe_2S_2(Cys)_3$ from the breaking of the Fe−N(His) bond observed in pathway 3. First, our AFM results showed several curves with a 2 nm force peak

https://dx.doi.org/10.1021/acs.analchem.0c03536
Anal. Chem. 2020, 92, 14783−14789

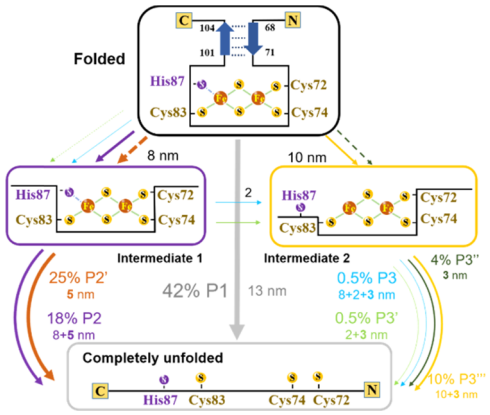


Figure 4. Schematic representation of the dynamic unfolding process of mNT showing three different types of unfolding pathways. P1 is the one-step unfolding of mNT with a single 13 nm peak. P2 is the two-step unfolding with a stepwise 8 nm peak and 5 nm peak, while P2′ only shows the 5 nm peak from the rupture of the intact 2Fe2S cluster. P3 is the three-step unfolding, showing a stepwise 8 nm peak, 2 nm peak, and 3 nm peak. It involves the rupture of a partially broken 2Fe2S$(Cys)_3$ cluster intermediate without the Fe−N(His) bond as the 3 nm peak. Similar P3′, P3″, and P3‴ were also observed. Each unfolding sequence is depicted by a specific colored arrow, the width of the line corresponds to the frequency of the pathway, and the dashed line indicates that the process is undetected.

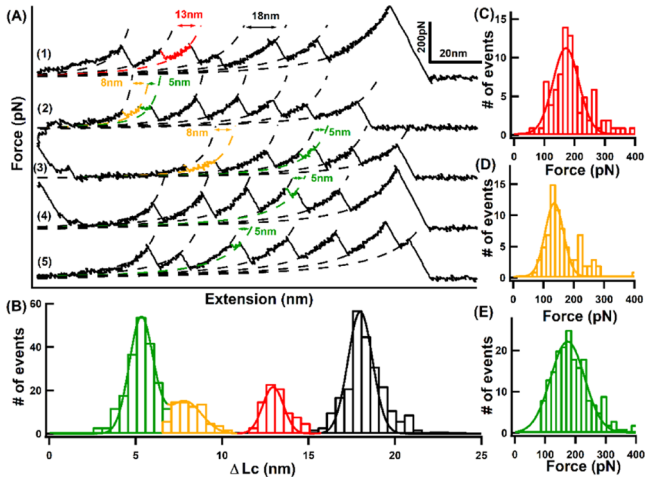


Figure 5. (A) Unfolding of H87C-mNT showing three major types of force−extension curves, similar to the results in Figure 3. A single 13 nm peak from mNT; a stepwise 8 and 5 nm peak, and a single 5 nm peak. The previous 2 and 3 nm peaks from the stepwise rupture of the 2Fe2S cluster mostly disappeared. (B) ΔL_c histogram showing the three different peaks from mNT. Histograms of the unfolding/rupture force for mNT (C), the 8 nm peak (D), and the 2Fe2S cluster (E) are shown.

(P3 + P3′, 1%, n = 14), indicating that the breaking of the single Fe−N bond can be independent of the breaking of the remaining cluster $Fe_2S_2(Cys)_3$. Although this number of events is too low for a solid conclusion, more than one hundred curves showed the other two similar rupture pathways (P3″ + P3‴, 14%, n = 130), leading to a convincing conclusion. Taken together, this pathway suggested that the rupture event of the Fe(III)−N(His) bond was too weak to be observed, verifying the lability of this unique Fe−N(His) bond, and demonstrated the presence of a partially ruptured metal cluster intermediate $Fe_2S_2(Cys)_3$.

It is noted that this single histidine ligand for the metal cluster forming a Fe−N(His) bond in mNT is one of the essential features of NEET proteins; all three NEET proteins discovered to date share this unique cluster. Previous studies have shown that this Fe−N(His) bond is responsible for metal cluster transfer to other Fe_2S_2 protein acceptors.[6] This feature is critical for its potential function in iron and metal cluster hemostasis. Here, our result showed that the Fe−N(His) bond is weak whose rupture leads to a partially ruptured 2Fe2S cluster intermediate, $Fe_2S_2(Cys)_3$. This remaining three-ligand coordinated intermediate is still an intact 2Fe2S cluster.

To further verify that this labile Fe−N bond is responsible for the $Fe_2S_2(Cys)_3$ intermediate, we constructed an H87C-mNT variant whose iron-coordinating histidine is mutated to cysteine. Based on our hypothesis, this cysteine will stabilize the cluster and reduce the presence of the $Fe_2S_2(Cys)_3$ intermediate. Indeed, AFM measurements on the $(GB1)_3$-H87C-mNT-$(GB1)_3$ polyprotein showed the 13 nm peak, 8 nm peak, and 5 nm peak with a higher unfolding force of 163 ± 60 (n = 88), 128 + 43 (n = 79), and 166 ± 79 pN (n = 194), respectively (Figure 5). However, the 3 nm peak and 2 nm peak, which were from the stepwise rupture of the cluster, mostly disappeared. Thus, this corroborates our conclusion that His87 makes the cluster dynamic and leads to the formation of intermediate 2. It is noted that this intermediate 2 from the rupture of the Fe−N(His87) bond is detected during our mechanical unfolding process of mNT. This process is different from the classical chemical or thermal protein unfolding and kinetic competing experiment between proteins. Thus, their results are not necessarily the same. Nevertheless, previous metal cluster competing studies on mNT found that this H87C-mNT mutant inhibited transfer of the metal cluster to the iron acceptor protein, suggesting that this intermediate may play a role in the metal transfer process.

Previous AFM-SMFS work on other iron−sulfur proteins supports our conclusion. Ferredoxin from cyanobacteria *Anabaena* contains the same 2Fe2S cluster as mNT but is coordinated by cysteine as $Fe_2S_2(Cys)_4$.[45] Compared to their rupture force (240 vs 80 pN, 400 nm/s) and unfolding rate k_{off} (0.07 vs 0.68 s^{-1}), the $Fe_2S_2(His)_1(Cys)_3$ cluster in mNT is much weaker and labile. Moreover, there is no rupture intermediate of the 2Fe2S cluster observed in the ferredoxin unfolding experiment. Similar results are found in our H87C-mNT mutant. Additional evidence can be found from a high-potential iron−sulfur protein from *chromatium tepidum* (cHiPIP).[46] cHiPIP contains a 4Fe4S cluster, which is also coordinated by cysteines as a $Fe_4S_4(Cys)_4$ cluster. The AFM result showed that its cluster is more stable with a rupture force of 179 pN (oxidized form, 400 nm/s) and an off rate of 0.39 s^{-1}. These results further indicate a labile 2Fe2S cluster in mNT due to the presence of the Fe−N bond. Nevertheless, it is noted that we worked on an mNT monomer which is less structured than the dimer, which may further weaken the cluster. In addition, the typical asymmetrical force distribution with a low force tail for the two-state proteins unfolding was not observed for many rupture events here. This is perhaps due to the multiple metal−ligand bond feature (three Fe−S bonds and one Fe−N bond) of the cluster in mNT. Normally, the rupture of the Fe−N(His87) bond and the Fe−S(Cys87) bond is enough for the unfolding and extension of the metal cluster binding motif. But the four metal−ligand bonds may break simultaneously, leading to a different force distribution with a high force tail sometimes.

https://dx.doi.org/10.1021/acs.analchem.0c03536
Anal. Chem. 2020, 92, 14783−14789

Thanks to the development of the single-molecule technique and theoretical model, many (un)folding intermediates of protein have been identified.[12,55−57] And the partially ruptured metal center/cluster is observed with increasing examples.[10,40] Here, we added another example, which is a functionally metal cluster intermediate, by studying the unique $Fe_2S_2(His)_1(Cys)_3$ cluster in mNT using AFM-SMFS. Our work not only demonstrates the powerful ability of SMFS to study proteins but also provides molecular information on how the unique Fe−N bond modulates the metal cluster and protein.

MATERIALS AND METHODS

Protein Engineering. The plasmid encoding the soluble cytoplasmic part (residues 33−108) of human mitoNEET was purchased from Genscript. The mNT-His87Cys variant was built by the standard site-directed mutagenesis method. The gene for the polyprotein, $(GB1)_3$-mNT-$(GB1)_3$, was subcloned into the pQE80L vector using standard molecular biology techniques and subsequently overexpressed in BL21(DE3) *Escherichia coli* cells. The cells were cultured in M9 minimal medium, and protein expression was induced for 18 h at 23 °C by the addition of 1 mM IPTG and 1 mM $FeCl_3$ (final concentration). The subsequent protein purification and characterization are described in the Supporting Information.

Apo-mNT Preparation. Apo-mNT was prepared using an established procedure with the iron-depleting agent, ethylenediaminetetraacetic acid (EDTA), and the cysteine-blocking agent, *N*-ethylmaleimide (NEM), under acidic conditions.[6,8] As a result, the protein solution became colorless and the characteristic absorption at 458 nm from the cluster vanished (Figure S2).

AFM-SMFS. Single-molecule AFM experiments were carried out using a commercial atomic force microscope (Nanowizard 4, JPK). A Si_3N_4 cantilever (MLCT, Bruker) was used and calibrated in Tris buffer (50 mM, pH 7.4) before each experiment, yielding a spring constant of ∼50 pN/nm. Approximately 10 μL of the protein sample, at a concentration of ∼0.5 mg/mL, was deposited onto a clean glass coverslip and incubated for 30 min at 25 °C following the addition of 1.5 mL of Tris buffer. Experiments were performed under a constant pulling velocity of 400 nm/s at 25 °C if not specified.

During the experiment, the polyprotein was deposited and nonspecifically absorbed on the glass coverslip. Subsequently, the AFM tip was pressed against the glass with a typical indentation force of 600 pN and a surface dwell time of 100 ms to randomly pick up a polyprotein via a nonspecific interaction (Figure 1C). By moving the AFM tip vertically, mNT was stretched and unfolded, resulting in the rupture of the iron−sulfur cluster and the Fe−N bond. The pulling distance was 400 nm, and the sample rate was 8800 Hz. Finally, the molecule was detached, and the tip moved up for repeated cycles in another location. In total, we performed five successful, independent single-molecule unfolding experiments on wild-type holo-mNT under 400 nm/s. The curve attempts were 731 792 times with 2006 successful single-molecule pick-up events. The pick-up ratio was 0.3%. The force−extension curve was fitted by the WLC model using the following equation

$$F(x) = \frac{k_B T}{P}\left[\frac{1}{4}\left(1 - \frac{x}{L_c}\right)^{-2} - \frac{1}{4} + \frac{x}{L_c}\right] \quad (1)$$

where $F(x)$ is the force applied to the polymer (polypeptide chain) under a polymer extension x. P is the persistence length of the polymer. L_c is the contour length. k_B is the Boltzmann constant, and T is the temperature in kelvin. The average persistence length of mNT is ∼0.4 nm (Figure S8).

Bell−Evans Model to Extract Rupture Kinetics Based on the Loading Rate Experiment. The rupture of the iron−sulfur cluster in mNT is a nonequilibrium process that is modeled as an all-or-none two-state process with a force-dependent rate constant $k(F)$. The rate constant can be described by the Bell−Evans model[54]

$$k(F) = k_0 \exp\left(\frac{F\Delta x_\beta}{k_b T}\right) \quad (2)$$

where $k(F)$ is the unfolding/unbinding rate constant under a stretching force of F, k_b is the unfolding/unbinding rate constant at zero force, and Δx_β is the distance between the bonded state and the transition state.

For dynamic force spectroscopy measurements, the slope a of the force−extension curves immediately (∼3 nm) before the rupture event (Figure S9) was first determined to obtain the average loading rate ($r = av$, where v is the velocity in the rupture event). All data were fitted with the Bell−Evans model (2), thus yielding the spontaneous rupture rate and the distance from the bound state to the transition state with the following equation

$$F = \frac{k_B T}{\Delta x_\beta}\ln\left(\frac{\Delta x_\beta}{k_0 k_B T}\right) + \frac{k_B T}{\Delta x_\beta}\ln(r) \quad (3)$$

By performing the AFM unfolding experiment under five different pulling speeds, 200, 400, 1000, 2000, and 4000 nm/s, the relationship between the most probable rupture force and the loading rate can be obtained on a log scale, which is fitted by a linear line as eq 3. Thus, the slope of this line can be used to calculate the Δx_β, which is the distance between the bonded state and the transition state, and the y-intercept is used to calculate the k_0.

ASSOCIATED CONTENT

Supporting Information

The Supporting Information is available free of charge at https://pubs.acs.org/doi/10.1021/acs.analchem.0c03536.

Protein purification; apo-mNT preparation; mass spectroscopy; protein sequence; schematic of the mNT monomer and dimer; gel filtration and SDS-PAGE of mNT; CD spectra of apo and holo-mNT; persistence length histogram of mNT; and method for calculating the loading rate of a rupture event (PDF)

AUTHOR INFORMATION

Corresponding Author

Peng Zheng − *State Key Laboratory of Coordination Chemistry, Chemistry and Biomedicine Innovation Center, School of Chemistry and Chemical Engineering, Nanjing University, Nanjing, Jiangsu 210023, P. R. China*; Email: pengz@nju.edu.cn

Authors

Guobin Song − *State Key Laboratory of Coordination Chemistry, Chemistry and Biomedicine Innovation Center,*

https://dx.doi.org/10.1021/acs.analchem.0c03536
Anal. Chem. 2020, 92, 14783−14789

School of Chemistry and Chemical Engineering, Nanjing University, Nanjing, Jiangsu 210023, P. R. China

Xuan Ding − *State Key Laboratory of Analytical Chemistry for Life Science, School of Chemistry and Chemical Engineering, Nanjing University, Nanjing, Jiangsu 210023, P. R. China*

Huaxing Liu − *State Key Laboratory of Coordination Chemistry, Chemistry and Biomedicine Innovation Center, School of Chemistry and Chemical Engineering, Nanjing University, Nanjing, Jiangsu 210023, P. R. China*

Guodong Yuan − *State Key Laboratory of Coordination Chemistry, Chemistry and Biomedicine Innovation Center, School of Chemistry and Chemical Engineering, Nanjing University, Nanjing, Jiangsu 210023, P. R. China*

Fang Tian − *State Key Laboratory of Coordination Chemistry, Chemistry and Biomedicine Innovation Center, School of Chemistry and Chemical Engineering, Nanjing University, Nanjing, Jiangsu 210023, P. R. China*

Shengchao Shi − *State Key Laboratory of Coordination Chemistry, Chemistry and Biomedicine Innovation Center, School of Chemistry and Chemical Engineering, Nanjing University, Nanjing, Jiangsu 210023, P. R. China*

Yang Yang − *State Key Laboratory of Coordination Chemistry, Chemistry and Biomedicine Innovation Center, School of Chemistry and Chemical Engineering, Nanjing University, Nanjing, Jiangsu 210023, P. R. China*

Guoqiang Li − *State Key Laboratory of Coordination Chemistry, Chemistry and Biomedicine Innovation Center, School of Chemistry and Chemical Engineering, Nanjing University, Nanjing, Jiangsu 210023, P. R. China*

Complete contact information is available at: https://pubs.acs.org/10.1021/acs.analchem.0c03536

Author Contributions

G.S., X.D., G.L., H.L., and G.Y. performed the experiments; G.S., X.D., F.T., and S.S analyzed the data and prepared the figures; P.Z. and G.S. wrote the manuscript.

Notes

The authors declare no competing financial interest.

■ ACKNOWLEDGMENTS

This work was supported by the National Natural Science Foundation of China (Grant Nos. 21771103, 21977047) and the Fundamental Research Funds for the Central Universities (14380205). We are grateful to the High Performance Computing Center (HPCC) of Nanjing University for doing the numerical calculations in this paper on its blade cluster system.We thank all anonymous reviewers for their advice and comments.

■ REFERENCES

(1) Beinert, H.; Holm, R. H.; Münck, E. *Science* **1997**, *277*, 653.
(2) Liu, J.; Chakraborty, S.; Hosseinzadeh, P.; Yu, Y.; Tian, S.; Petrik, I.; Bhagi, A.; Lu, Y. *Chem. Rev.* **2014**, *114*, 4366.
(3) Karmi, O.; Marjault, H.-B.; Pesce, L.; Carloni, P.; Onuchic, J. N.; Jennings, P. A.; Mittler, R.; Nechushtai, R. *J. Biol. Inorg. Chem.* **2018**, *23*, 599.
(4) Geldenhuys, W. J.; Leeper, T. C.; Carroll, R. *Drug Discovery Today* **2014**, *19*, 1601.
(5) Paddock, M. L.; Wiley, S. E.; Axelrod, H. L.; Cohen, A. E.; Roy, M.; Abresch, E. C.; Capraro, D.; Murphy, A. N.; Nechushtai, R.; Dixon, J. E.; Jennings, P. A. *Proc. Natl. Acad. Sci. U.S.A.* **2007**, *104*, 14342.
(6) Zuris, J. A.; Harir, Y.; Conlan, A. R.; Shvartsman, M.; Michaeli, D.; Tamir, S.; Paddock, M. L.; Onuchic, J. N.; Mittler, R.; Cabantchik, Z. I.; Jennings, P. A.; Nechushtai, R. *Proc. Natl. Acad. Sci. U.S.A.* **2011**, *108*, 13047.
(7) Tan, G.; Liu, D.; Pan, F.; Zhao, J.; Li, T.; Ma, Y.; Shen, B.; Lyu, J. *Biochem. Biophys. Res. Commun.* **2016**, *470*, 226.
(8) Hou, X.; Liu, R.; Ross, S.; Smart, E. J.; Zhu, H.; Gong, W. *J. Biol. Chem.* **2007**, *282*, 33242.
(9) Tapia-Rojo, R.; Eckels, E. C.; Fernández, J. M. *Proc. Natl. Acad. Sci. U.S.A.* **2019**, *116*, 7873.
(10) Mojumdar, S. S.; Scholl, Z. N.; Dee, D. R.; Rouleau, L.; Anand, U.; Garen, C.; Woodside, M. T. *Nat. Commun.* **2017**, *8*, No. 1881.
(11) Suren, T.; Rutz, D.; Mossmer, P.; Merkel, U.; Buchner, J.; Rief, M. *Proc. Natl. Acad. Sci. U.S.A.* **2018**, *115*, 11688.
(12) Cecconi, C.; Shank, E. A.; Bustamante, C.; Marqusee, S. *Science* **2005**, *309*, 2057.
(13) Mondal, J.; Halverson, D.; Li, I. T.; Stirnemann, G.; Walker, G. C.; Berne, B. J. *Proc. Natl. Acad. Sci. U.S.A.* **2015**, *112*, 9270.
(14) Pei, Y.; Liu, Y.; Xie, C.; Zhang, X.; You, H. *Anal. Chem.* **2020**, *92*, 4504.
(15) Senapati, S.; Poma, A. B.; Cieplak, M.; Filipek, S.; Park, P. S. H. *Anal. Chem.* **2019**, *91*, 7226.
(16) Zheng, Y.; Geng, X.; Yang, X.; Li, S.; Liu, Y.; Liu, X.; Wang, Q.; Wang, K.; Jia, R.; Xu, Y. *Anal. Chem.* **2020**, *92*, 2853.
(17) Xing, H.; Li, Z.; Wang, W.; Liu, P.; Liu, J.; Song, Y.; Wu, Z. L.; Zhang, W.; Huang, F. *CCS Chem.* **2020**, *2*, 513.
(18) Hoffmann, T.; Tych, K. M.; Crosskey, T.; Schiffrin, B.; Brockwell, D. J.; Dougan, L. *ACS Nano* **2015**, *9*, 8811.
(19) Walder, R.; Van Patten, W. J.; Ritchie, D. B.; Montange, R. K.; Miller, T. W.; Woodside, M. T.; Perkins, T. T. *Nano Lett.* **2018**, *18*, 6318.
(20) Giganti, D.; Yan, K.; Badilla, C. L.; Fernandez, J. M.; Alegre-Cebollada, J. *Nat. Commun.* **2018**, *9*, No. 185.
(21) Scholl, Z. N.; Yang, W.; Marszalek, P. E. *ACS Nano* **2015**, *9*, 1189.
(22) Alonso-Caballero, A.; Schönfelder, J.; Poly, S.; Corsetti, F.; De Sancho, D.; Artacho, E.; Perez-Jimenez, R. *Nat. Commun.* **2018**, *9*, No. 2758.
(23) Galera-Prat, A.; Moraïs, S.; Vazana, Y.; Bayer, E. A.; Carrión-Vázquez, M. *J. Biol. Chem.* **2018**, *293*, 7139.
(24) Goktas, M.; Luo, C.; Sullan, R. M. A.; Bergues-Pupo, A. E.; Lipowsky, R.; Vila Verde, A.; Blank, K. G. *Chem. Sci.* **2018**, *9*, 4610.
(25) Schönfelder, J.; Alonso-Caballero, A.; De Sancho, D.; Perez-Jimenez, R. *Chem. Soc. Rev.* **2018**, *47*, 3558.
(26) Fu, L.; Wang, H.; Li, H. *CCS Chem.* **2019**, *1*, 138.
(27) Takahashi, H.; Rico, F.; Chipot, C.; Scheuring, S. *ACS Nano* **2018**, *12*, 2719.
(28) Moy, V. T.; Florin, E. L.; Gaub, H. E. *Science* **1994**, *266*, 257.
(29) Kumar, K.; Woo, S. M.; Siu, T.; Cortopassi, W. A.; Duarte, F.; Paton, R. S. *Chem. Sci.* **2018**, *9*, 2655.
(30) Oh, Y. J.; Koehler, M.; Lee, Y.; Mishra, S.; Park, J. W.; Hinterdorfer, P. *Nano Lett.* **2019**, *19*, 612.
(31) Becke, T. D.; Ness, S.; Gurster, R.; Schilling, A. F.; di Guilmi, A. M.; Sudhop, S.; Hilleringmann, M.; Clausen-Schaumann, H. *ACS Nano* **2018**, *12*, 549.
(32) Wang, Y.; Barnett, S. F. H.; Le, S.; Guo, Z.; Zhong, X.; Kanchanawong, P.; Yan, J. *Nano Lett.* **2019**, *19*, 7514.
(33) Yoon, J.; Kim, Y.; Park, J. W. *Anal. Chem.* **2019**, *91*, 8422.
(34) Lyu, X.; Song, Y.; Feng, W.; Zhang, W. *ACS Macro Lett.* **2018**, *7*, 762.
(35) Zhang, S.; Qian, H.-j.; Liu, Z.; Ju, H.; Lu, Z.-y.; Zhang, H.; Chi, L.; Cui, S. *Angew. Chem., Int. Ed.* **2019**, *58*, 1659.
(36) Huang, W.; Wu, X.; Gao, X.; Yu, Y.; Lei, H.; Zhu, Z.; Shi, Y.; Chen, Y.; Qin, M.; Wang, W.; Cao, Y. *Nat. Chem.* **2019**, *11*, 310.
(37) Krieg, M.; Fläschner, G.; Alsteens, D.; Gaub, B. M.; Roos, W. H.; Wuite, G. J. L.; Gaub, H. E.; Gerber, C.; Dufrêne, Y. F.; Müller, D. J. *Nat. Rev. Phys.* **2019**, *1*, 41.
(38) Pill, M. F.; East, A. L. L.; Marx, D.; Beyer, M. K.; Clausen-Schaumann, H. *Angew. Chem., Int. Ed.* **2019**, *58*, 9787.

(39) Zhang, X.; Liu, C.; Wang, Z. *Polymer* **2008**, *49*, 3353.
(40) Beedle, A. E. M.; Lezamiz, A.; Stirnemann, G.; Garcia-Manyes, S. *Nat. Commun.* **2015**, *6*, No. 7894.
(41) Lin, Y.; Kouznetsova, T. B.; Craig, S. L. *J. Am. Chem. Soc.* **2020**, *142*, 2105.
(42) Leader, A.; Mandler, D.; Reches, M. *Phys. Chem. Chem. Phys.* **2018**, *20*, 29811.
(43) Mejía, L.; Franco, I. *Chem. Sci.* **2019**, *10*, 3249.
(44) Perales-Calvo, J.; Lezamiz, A.; Garcia-Manyes, S. *J. Phys. Chem. Lett.* **2015**, *6*, 3335.
(45) Lei, H.; Guo, Y.; Hu, X.; Hu, C.; Hu, X.; Li, H. *J. Am. Chem. Soc.* **2017**, *139*, 1538.
(46) Li, J.; Li, H. *J. Phys. Chem. B* **2018**, *122*, 9340.
(47) Yuan, G.; Liu, H.; Ma, Q.; Li, X.; Nie, J.; Zuo, J.; Zheng, P. *J. Phys. Chem. Lett.* **2019**, *10*, 5428.
(48) Arantes, G. M.; Bhattacharjee, A.; Field, M. J. *Angew. Chem., Int. Ed.* **2013**, *52*, 8144.
(49) Zheng, P.; Arantes, G. M.; Field, M. J.; Li, H. *Nat. Commun.* **2015**, *6*, No. 7569.
(50) Yadav, A.; Paul, S.; Venkatramani, R.; Ainavarapu, S. R. K. *Sci. Rep.* **2018**, *8*, No. 1989.
(51) Xia, J.; Zuo, J.; Li, H. *Nanoscale* **2019**, *11*, 19791.
(52) Cao, Y.; Lam, C.; Wang, M.; Li, H. *Angew. Chem., Int. Ed.* **2006**, *45*, 642.
(53) Siggia, E. D.; Marko, J. F. *Macromolecules* **1995**, *28*, 8759.
(54) Evans, E.; Ritchie, K. *Biophys. J.* **1997**, *72*, 1541.
(55) Wolynes, P. G.; Onuchic, J. N.; Thirumalai, D. *Science* **1995**, *267*, 1619.
(56) Dudko, O. K.; Hummer, G.; Szabo, A. *Proc. Natl. Acad. Sci. U.S.A.* **2008**, *105*, 15755.
(57) Bernardi, R. C.; Durner, E.; Schoeler, C.; Malinowska, K. H.; Carvalho, B. G.; Bayer, E. A.; Luthey-Schulten, Z.; Gaub, H. E.; Nash, M. A. *J. Am. Chem. Soc.* **2019**, *141*, 14752.

https://dx.doi.org/10.1021/acs.analchem.0c03536
Anal. Chem. 2020, 92, 14783−14789